Supplementary Infromation

Facile and Scalable Approach to Develop Electrochemical Unzipping of Multi-walled Carbon Nanotubes to Graphene Nanoribbons

Dongjin Ko[a‡], Juhyung Choi[a‡], Bingyi Yan[a], Taejin Hwang[a], Xuanzhen Jin[b], Jong Min Kim[a], and Yuanzhe Piao[ac*]

[a] Department of Transdisciplinary Studies, Graduate School of Convergence Science and Technology, Seoul National University, 145 Gwanggyo-ro, Yeongtong-gu, Suwon-si, Gyeonggi-do 16229, Republic of Korea.

[b] Department of Polymer Materials and Engineering, Yanbian University, Yanji 133002, Jilin, P.R. China.

[c] Advanced Institutes of Convergence Technology, 145 Gwanggyo-ro, Yeongtong-gu, Suwon-si, Gyeonggi-do 16229, Republic of Korea.

‡ These authors contributed equally to this work.

List of Contents

1. Electrochemical synthesis at different condition in concentric sulfuric acid (18 M)

S1. Schematic explanation of a home-made zig set up.

S2. Electrochemical measurements of MWCNT at different mass loading in 18 M H_2SO_4.

S3. Electrochemical reactions of smaller diameter MWCNT were performed at 0.5 M and 18 M H_2SO_4.

S4. TEM images of GNRs: a-c) GNR-2.5H, d-f) GNR-4H, and g-i) GNR-7H, respectively.

S5. Material characterization of the unzipped MWCNT (denote as unzipped MWCNT-*i*).

S6. Cyclic voltammetry (CV) curves of MWCNTs and the obtained products at scan rate of 10 mV s^{-1}.

S7. High resolution XPS for C1s spectra of the as-prepared concentrated sulfuric acid products.

S8. Cell potential (V) versus Time (h) and Coulomb/mass loading.

2. Electrochemical reactions at different concentration of sulfuric acid

S9. Linear sweep voltammetry (LSV) curves of dilute H_2SO_4 electrolytes in the three-electrode cell at a scan rate of 0.5 mV s^{-1}.

S10. TEM images of the as-prepared products with caps; (a, d) 0.5 M Ox-MWNCT-7H, (b, e) 10 M Ox-MWNCT-7H, and (c, f) 15 M GNR-7H.

S11. Material characterization of the products obtained by electrochemical reactions at different concentrations of H_2SO_4.

3. Electrochemical applications of GNR-2.5H for hydrogen evolution reaction (HER)

S12. Brunauer–Emmett–Teller (BET) surface areas of MWCNT and GNR-2.5H.

S13. SEM images of the electrochemically exfoliated graphene (EEG); (a) Low and (b) High magnification.

S14. SEM images of (a) MoS_2, (b) MoS_2/EEG, (c) MoS_2/MWCNT, and (d) MoS_2/GNR-2.5H.

S15. TGA curves of MoS_2 and MoS_2/GNR-2.5H in air.

S16. Cyclic voltammograms (CV) of (a) MoS_2/GNR-2.5H, (b) MoS_2/MWCNT, and (c) MoS_2/EEG recorded at scan rates of 20 to 80 mV s^{-1}.

S17. Two CPE (constant phase element) equivalent circuit elements for the as-prepared catalysts.

Table S1. Comparison of electrochemical synthesis for unzipping the single or multi-walled carbon nanotube.

Table S2. The concentration of Fe element is determined by ICP-MS measurement.

Table S3. The full width at half maximum (FWHM) of the obtained products.

Table S4. The sheet resistance of the films was investigated by a four-point probe measurement.

Table S5. Comparison of reported experimental method with our electrochemical intercalation synthesis.

Electrochemical measurements

Measurements of hydrogen evolution reaction (HER);

The electrochemical performance was investigated using an electrochemical workstation (Metrohm Autolab workstation, PGSTAT 302N) in a standard three-electrode system. The glassy carbon rotating disk electrode (RDE) modified with samples, graphite rod, and Ag/AgCl (sat. KCl) was used as the working electrode, counter electrode, and reference electrode, respectively. The rotation speed of RDE was 2400 rpm. 5 mg of the sample for testing was dispersed in a mixture of deionized water (950 μL), followed by the addition of 5 wt% Nafion (50 μL, Aldrich). A homogeneous slurry was obtained by sonicating for 30 min. The dispersion (10 μL) was drop-casted on a glassy carbon electrode (GCE) and then dried using an infrared lamp. The mass loading of catalysts was 0.21 mg cm^{-2}. All measurements were calculated respect to reversible hydrogen electrode according to the Nernst equation S1: $E\ (V\ vs\ RHE) = E\ (V\ vs\ Ag/AgCl)\ + 0.197\ + 0.0591\ \times pH$The linear scan voltammetry (LSV) curve was measured at a scan rate of 2 mV s^{-1} in 0.5 M H_2SO_4. Double-layer capacitance was evaluated under a potential window of 0.2 to 0.3 V (vs. RHE) with various scan rates from 20 mV s^{-1} to 80 mV s^{-1} using CV in 0.5 M H_2SO_4. All LSV data were corrected with iR losses during the measurements.

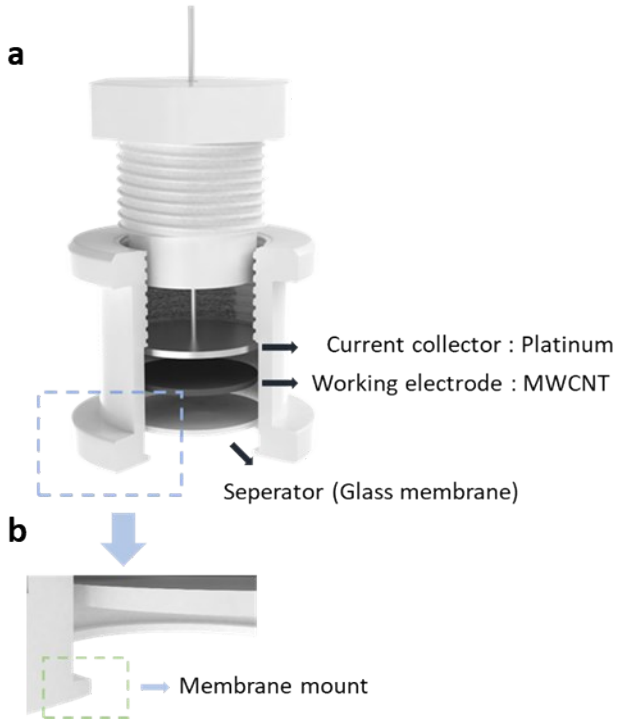

Figure S1. (a) The electrochemical apparatus consists of a cap (screw design), body, current collector (home-made platinum), working electrode (MWCNTs), and separator (glass fiber filter membrane was cut to fit the inside diameter (size: 20 mm) of the reactor). (b) Magnified view of the membrane mount used to support all parts of the reactor. In this design, the apparatus is made of PTFE because it shows excellent acid resistance in concentrated sulfuric acid.

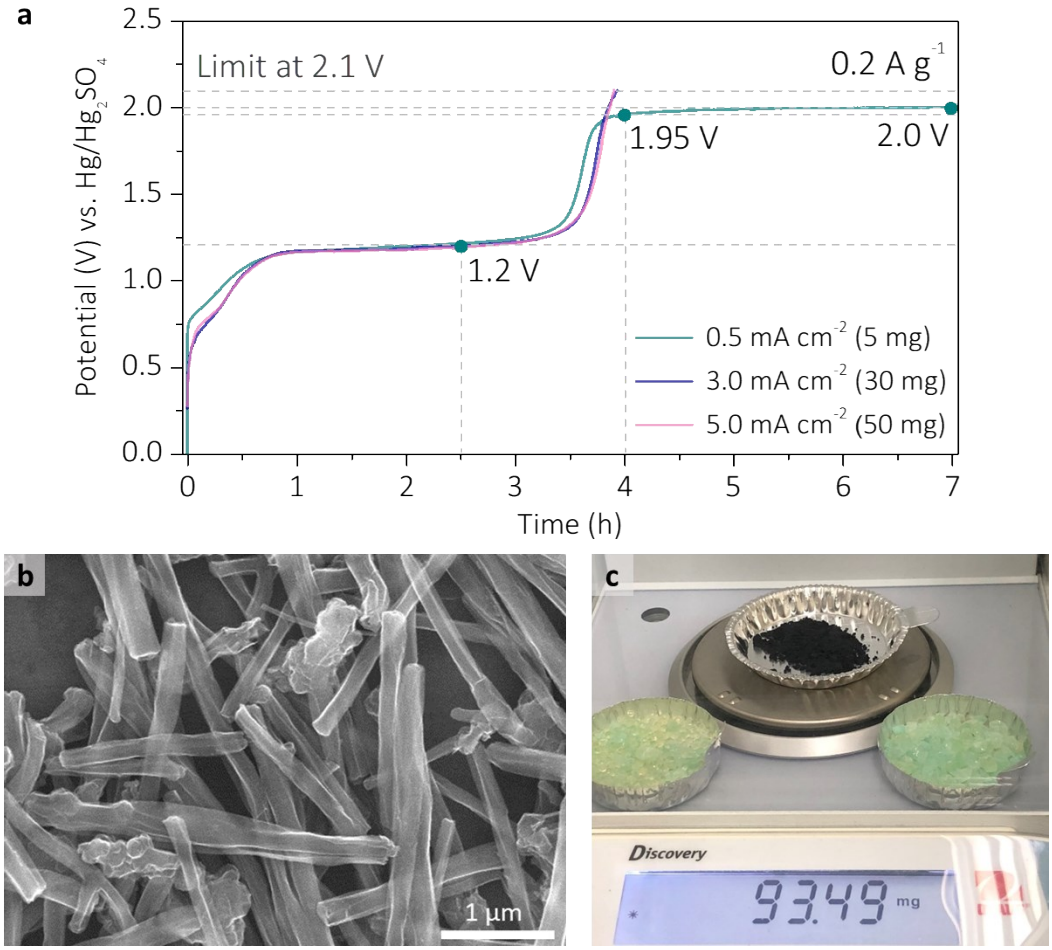

Figure S2. Electrochemical measurements of MWCNT in 18 M H_2SO_4. (a) Galvanostatic charging curve of MWCNT with a current density of 0.2 A g^{-1} in 18 M H_2SO_4 electrolyte at different mass loading. (b) SEM images obtained after electrochemical reaction for 2.5 hours and (c) Milligram-scale synthesis of GNR-2.5H was done in the laboratory.

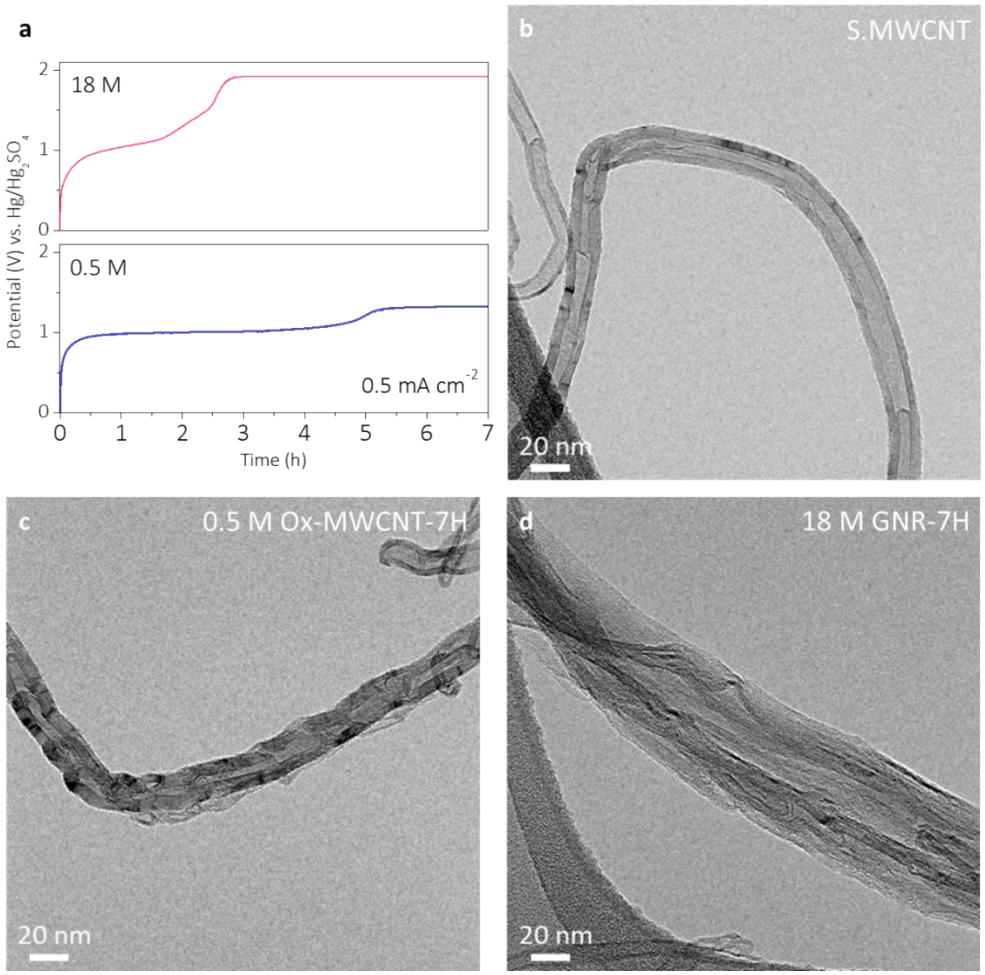

Figure S3. To confirm the synthesis of GNR with smaller diameter MWCNT, electrochemical reactions were performed at 0.5 M and 18 M H_2SO_4 electrolytes respectively. (a) Galvanostatic charge curve at current density of 0.5 mA cm^{-2}, (b) TEM images of pristine S-MWCNT, (c) surface oxidation of S-MWNCT performed in 0.5 M H_2SO_4 electrolyte, and (d) partially unzipped GNR performed in 18 M H_2SO_4 electrolyte.

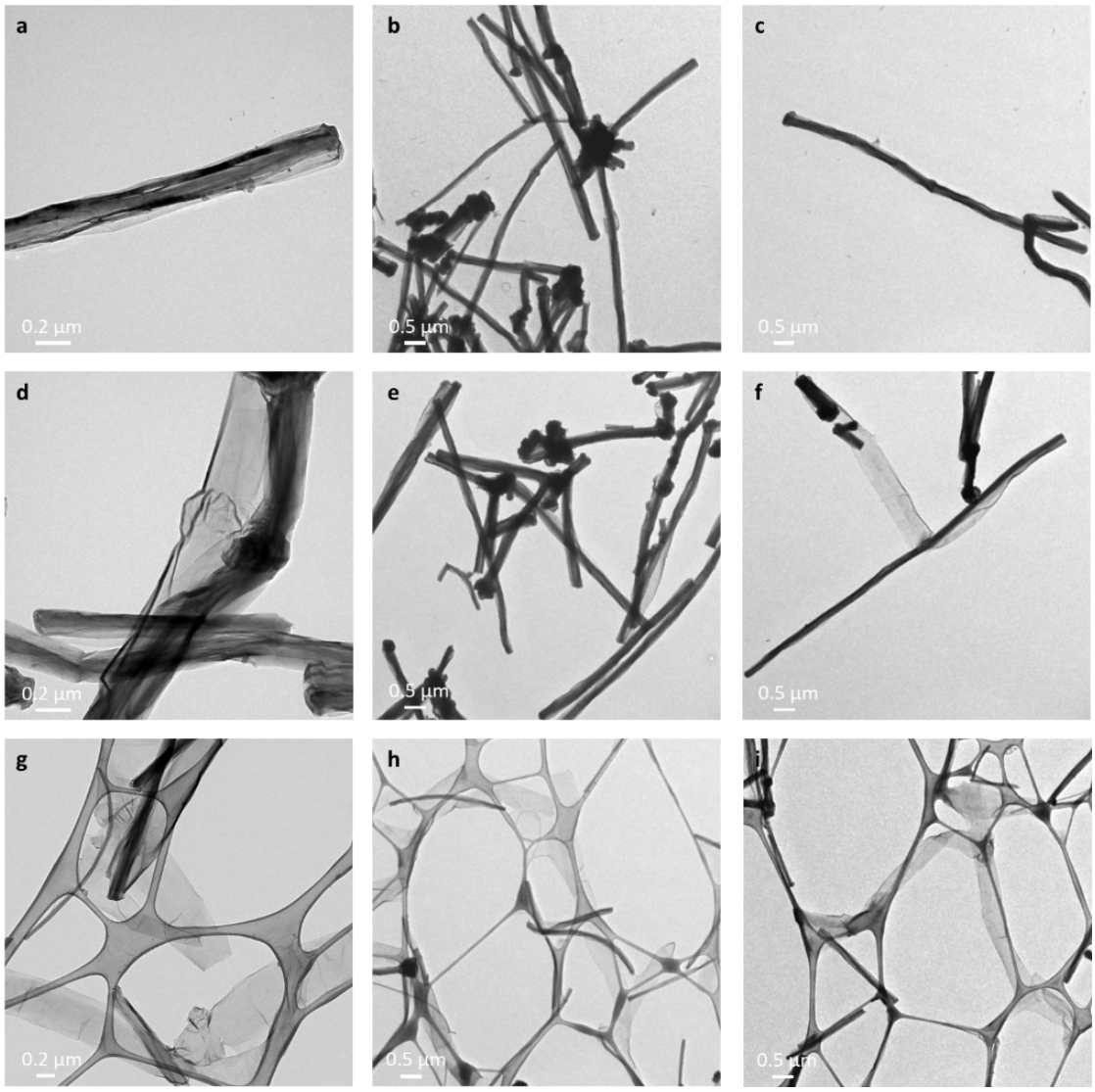

Figure S4. TEM images of GNRs: a-c) GNR-2.5H, d-f) GNR-4H, and g-i) GNR-7H, respectively.

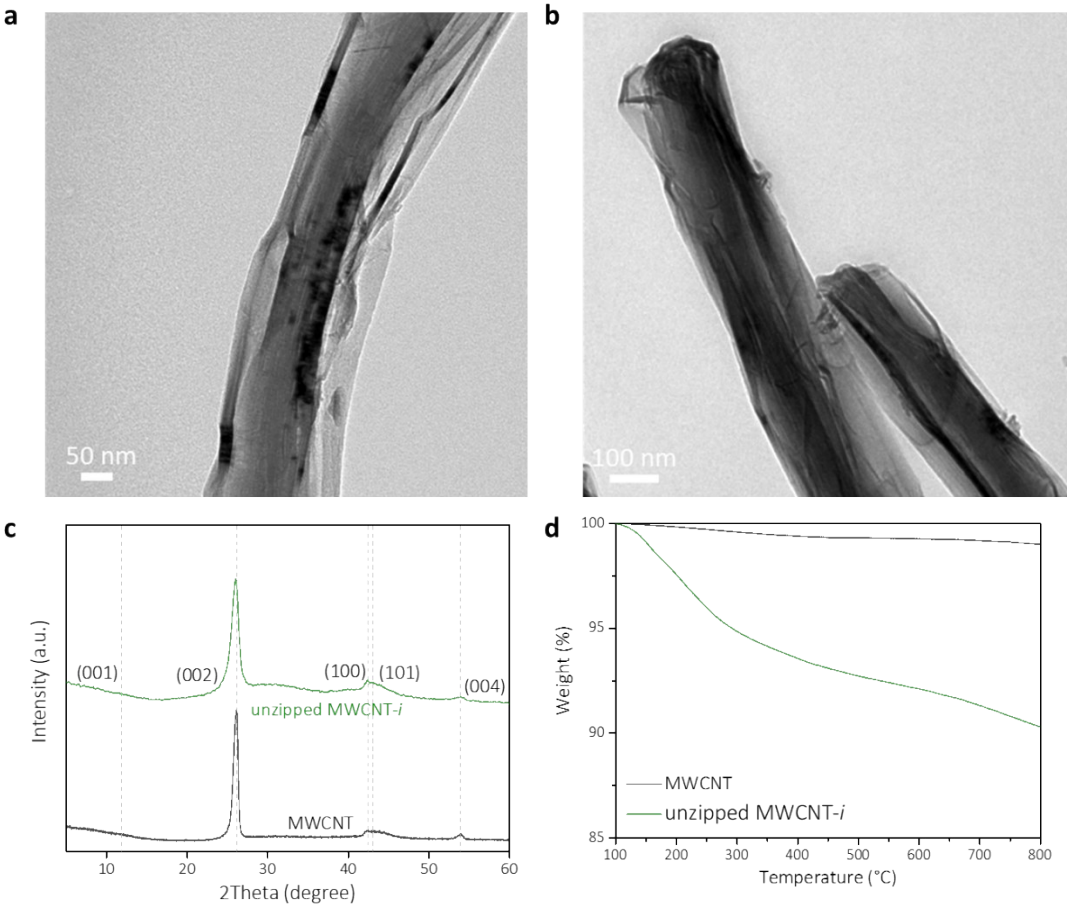

Figure S5. Material characterizations of the unzipped MWCNT (denote as unzipped MWCNT-*i*). (a, b) TEM images, (c) XRD patterns, and (d) TGA curves. The weight loss of unzipped MWCNT-*i* observed at 800 °C is approximately 9.7 wt%.

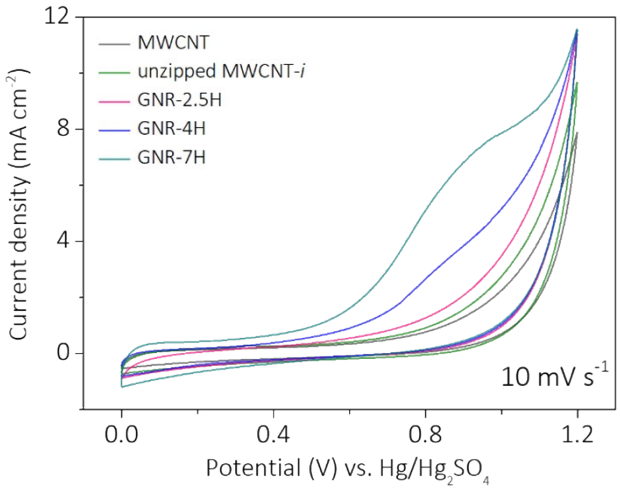

Figure S6. Cyclic voltammetry (CV) curves of MWCNTs and the obtained products at scan rate of 10 mV s^{-1}.

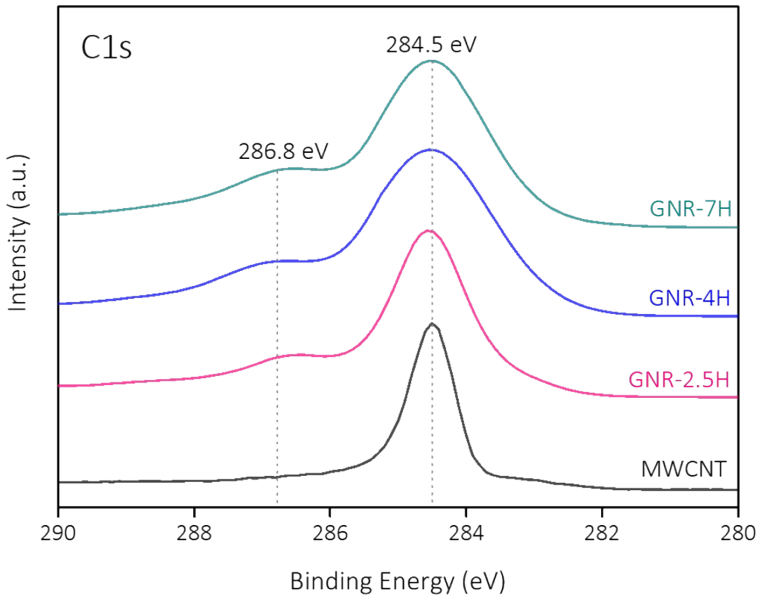

Figure S7. High resolution XPS for C1s spectra of the as-prepared concentrated sulfuric acid (18 M H_2SO_4) products.

The calculation of GIC stages for the galvanostatic charging curve in concentrated sulfuric acid

GIC consists of intercalant atomic or molecular layers inserted between graphene layers. The stage index n of graphite intercalation compounds is classified as n graphene layers separating successive intercalate layers. The chemical formula for GIC is $C_P^+ \cdot HSO_4^- \cdot H_2SO_4$ where the value of p is a measure of the charged carbon. To add, the phase range of p is related to the electrochemical charge (Q) and the mass loading (M) of the working electrode. For example, $p > 21$ is defined as stage index n (stage-1 GIC: $C_{21-28}^+ \cdot HSO_4^- \cdot H_2SO_4$). Based on an electrochemical intercalation reaction, the value of p can be calculated according to the following equation S2: $p = e \times M/m_a \times Q$, where e (C) is the electric charge, M is the mass loading of the working electrode and m_a (g) is the atomic mass of carbon ($e/m_a = 8041\ C\ g^{-1}$).[S1]

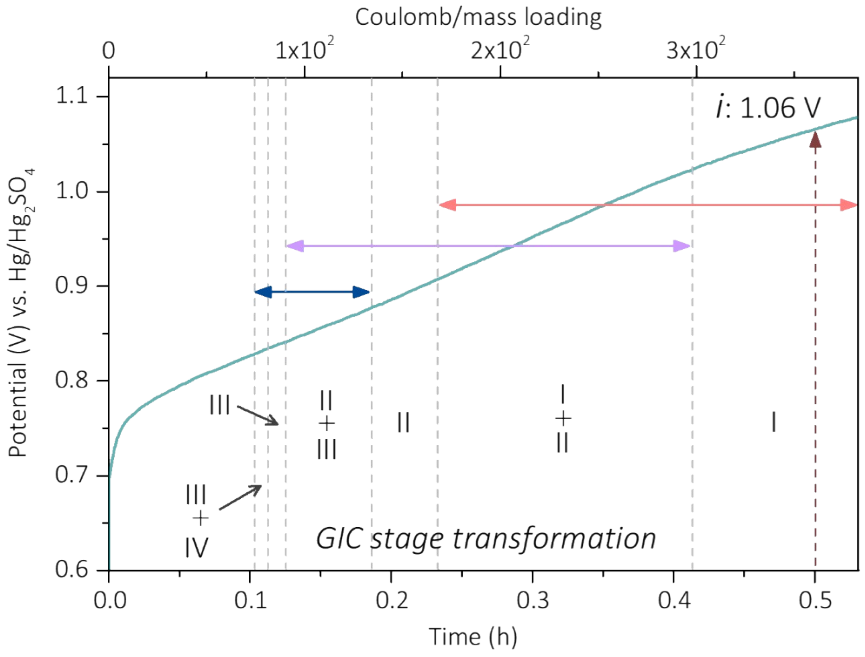

Figure S8. Cell potential (V) versus Time (h) and Coulomb/mass loading (The dashed lines indicating the GIC stage steps is calculated for the equation S2).

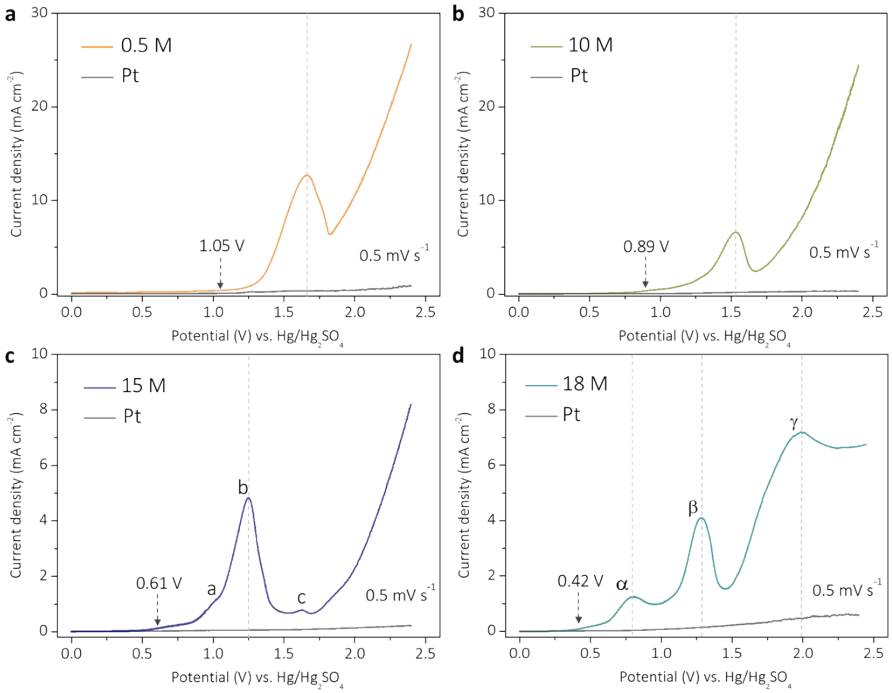

Figure S9. Linear sweep voltammetry (LSV) curves of dilute H_2SO_4 electrolytes in the three-electrode cell at a scan rate of 0.5 mV s^{-1}: (a) 0.5 M H_2SO_4, (b) 10 M H_2SO_4, (c) 15 M H_2SO_4, and (d) 18 M H_2SO_4. LSV curves of Pt (dotted line) were performed as a working electrode without MWCNT in the same electrochemical condition. In Figure S7a, a peak with a dashed line at ~ 1.66 V is corresponding to the surface oxidation and no other peak is shown. A first peak at ~ 0.89 V in Figure S7b is probably related to the intercalation of graphene layers with the co-intercalated water molecule. A second peak at ~1.53 V may refer to the formation of C-OH groups and further oxidation to carbonyls groups.[S2] LSV curves in Figure S7c and d, peak "a" at ~ 1.01 V and peak "α" at ~ 0.8 V show the electrochemical formation of the stage-1 GIC. The second peak "b" at ~ 1.25 V and "β" at ~ 1.28 V is probably due to the peroxidation of bisulfate anion.[S3] However, "c" peak at ~1.63 V and "γ" peak at ~ 1.99 V differ in the shapes, which may be due to the concentration of water in each H_2SO_4 electrolyte during the overoxidation reaction. All LSV curves show water decomposition in H_2SO_4 electrolytes when the potential becomes 2 V (V *vs.* Hg/Hg_2SO_4).

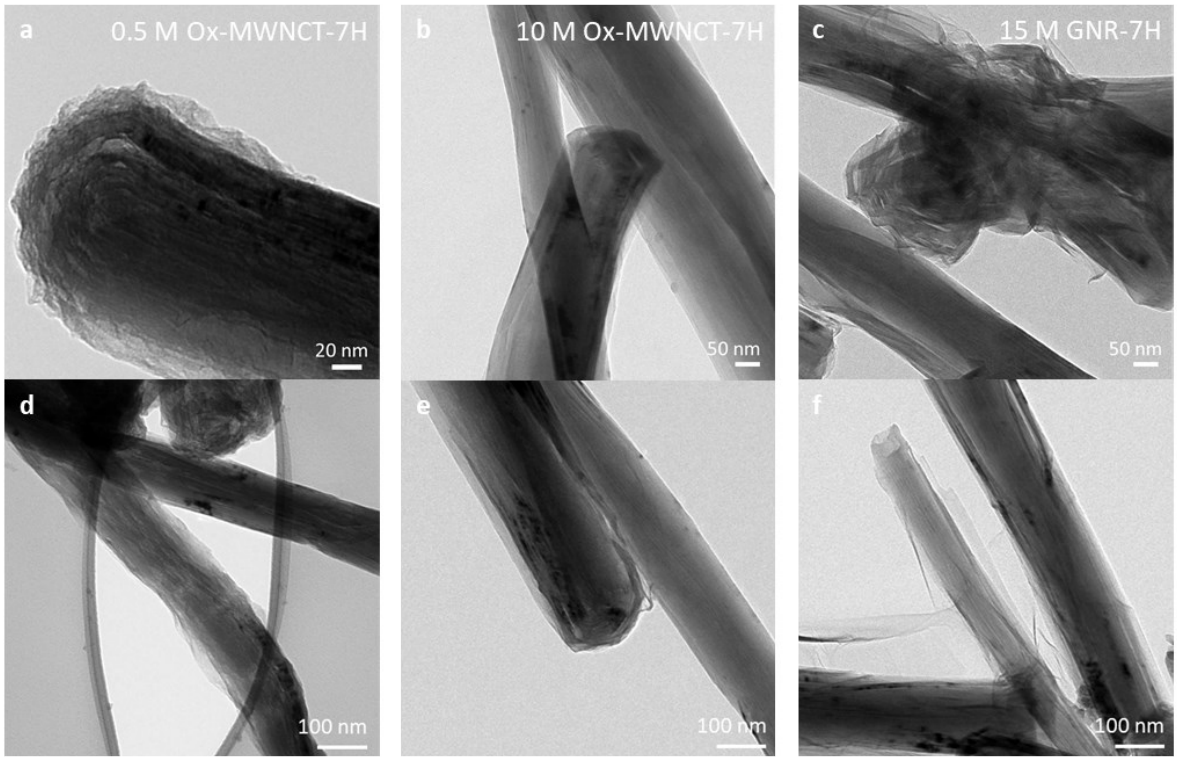

Figure S10. TEM images of the as-prepared products with caps; (a, d) 0.5 M Ox-MWNCT-7H, (b, e) 10 M Ox-MWNCT-7H, and (c, f) 15 M GNR-7H.

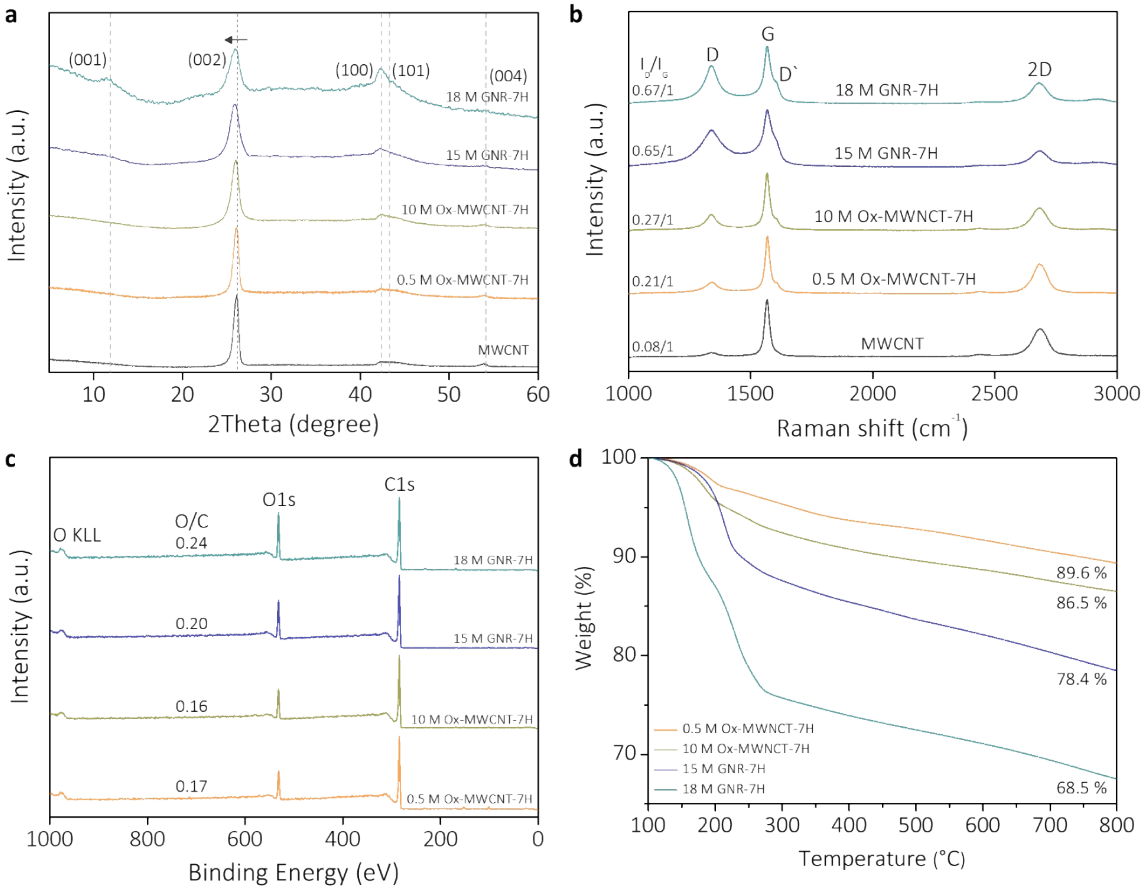

Figure S11. Characterization of the products obtained by electrochemical reactions at different concentrations of H_2SO_4. (a) X-ray diffraction, (b) Raman spectra, (c) XPS spectra, and (d) TGA with a ramping rate of 10 ˚C min^{-1} in N_2.

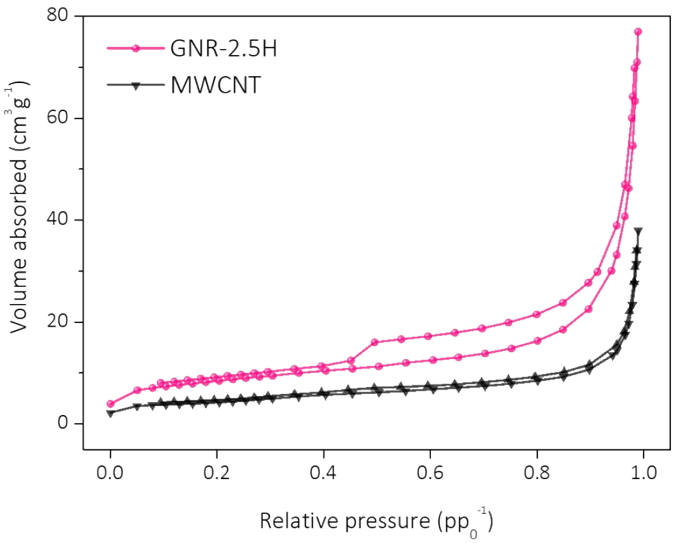

Figure S12. Brunauer–Emmett–Teller (BET) surface areas of MWCNT and GNR-2.5H.

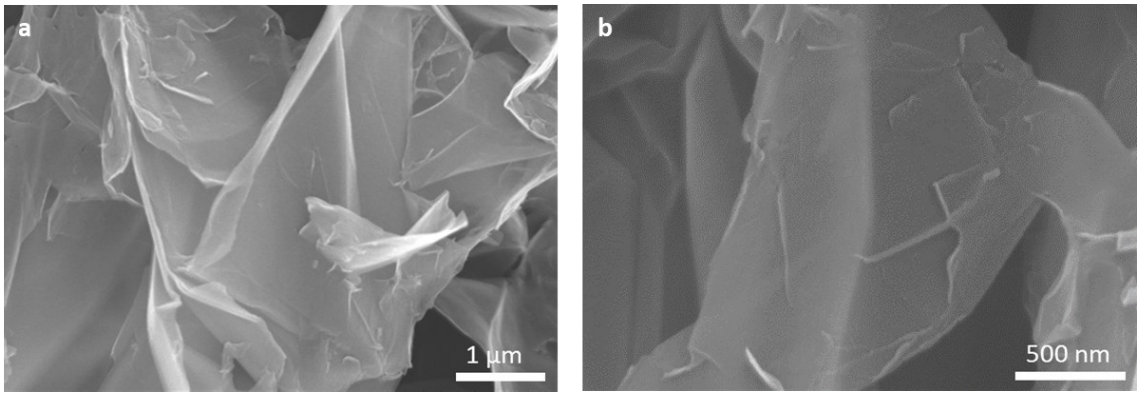

Figure S13. SEM images of the electrochemically exfoliated graphene (EEG); (a) Low and (b) High magnification.

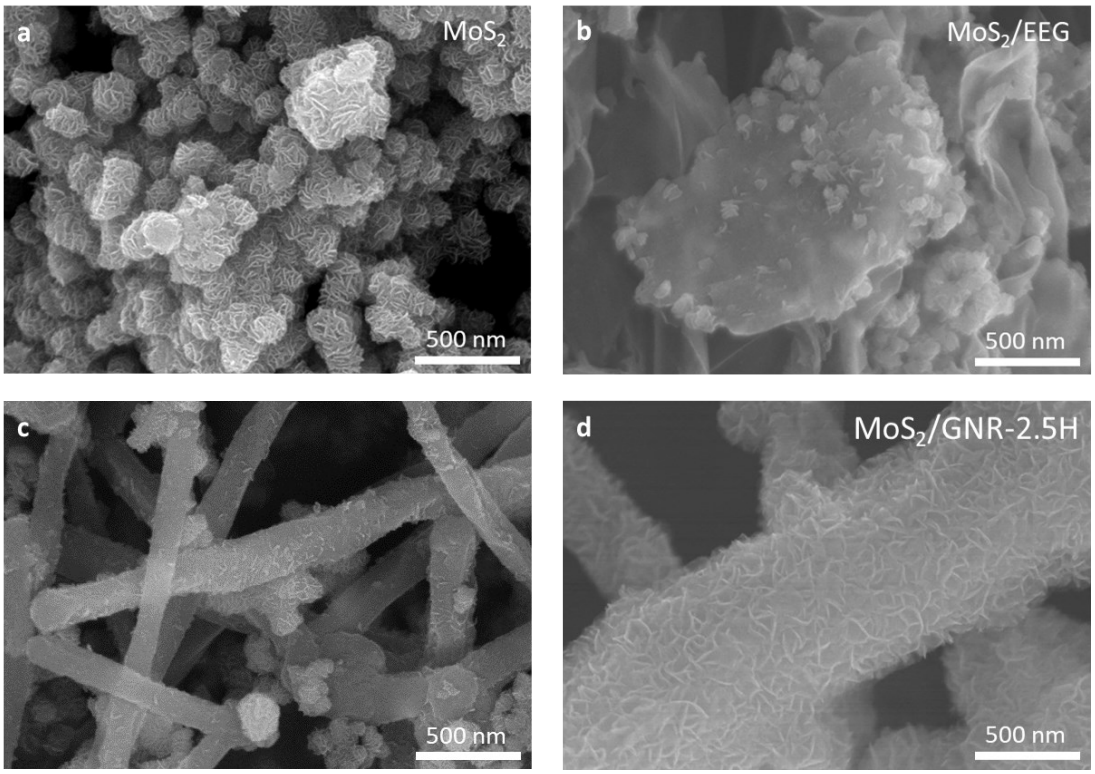

Figure S14. SEM images of (a) MoS_2, (b) MoS_2/EEG, (c) MoS_2/MWCNT, and (d) MoS_2/GNR-2.5H.

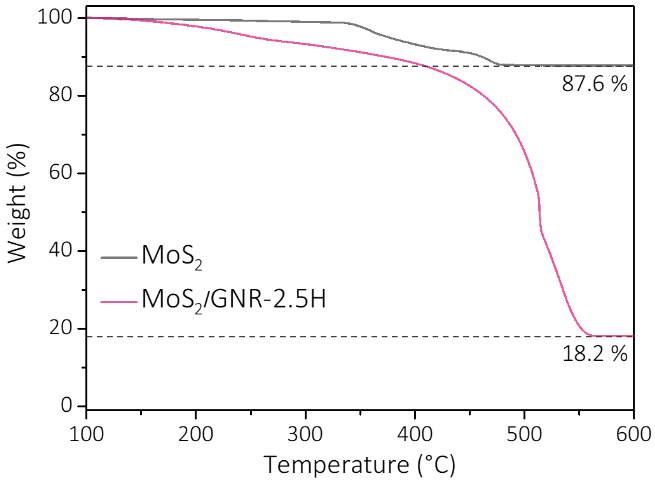

Figure S15. TGA curves of MoS_2 and MoS_2/GNR-2.5H in air. To determine Mo content in the MoS_2/GNR-2.5H, thermogravimetric analysis (TGA) and inductively coupled plasma atomic emission spectroscopy (ICP-AES) analysis were conducted. Concerning TGA results, the remaining mass percentage is 87.6% and 18.2% for MoS_2 and MoS_2/GNR-2.5H, respectively. Assuming a complete conversion of MoS_2 to MoO_3 and that of C to CO_2, it can be calculated that the mass percentage of Mo in these two products is 58.4% and 12.1%, respectively. Also, ICP-AES of the MoS_2/GNR-2.5H confirms that the mass percentage of Mo is 11%, which is close to the result of TGA analysis.

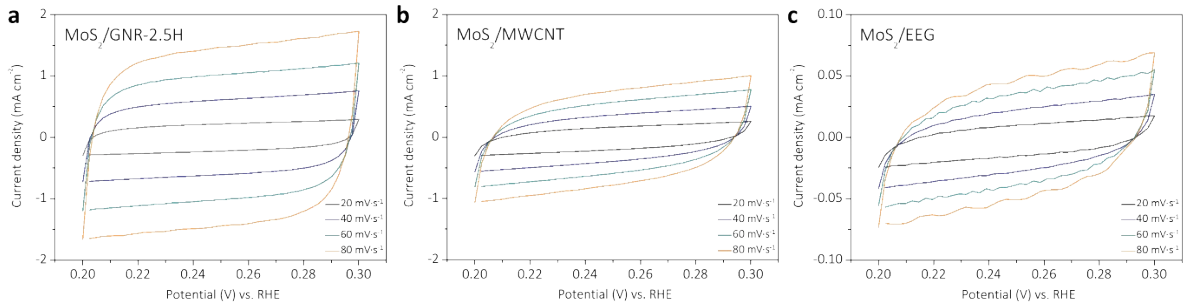

Figure S16. Cyclic voltammograms (CV) of (a) MoS_2/GNR-2.5H, (b) MoS_2/MWCNT, and (c) MoS_2/EEG recorded at scan rates of 20 to 80 mV s^{-1}.

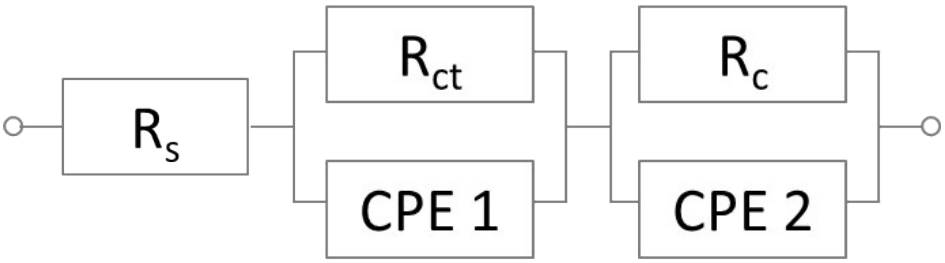

R_s = The series of electrolyte and contact resistance

R_{ct} = Charge-transfer resistance at the catalyst/solution interface

R_c = The resistance arises from solid/electrolyte interface

Figure S17. Two CPE (constant phase element) equivalent circuit elements for the as-prepared catalysts.

Table S1. Comparison of electrochemical synthesis for unzipping the single or multi-walled carbon nanotube.

Types of CNT	Mechanism	Working electrode	Reagents	Scalability (mass loading)	Ref
Single or Multi-walled carbon nanotube	Oxidative cleavage of the C-C bond	GCE[a)] (Drop casting)	0.5 M H_2SO_4	Difficult (2.5 μg)	[S4]
Multi-walled carbon nanotube	Hetero atom dopant-specific unzipping	GCE[a)] (CNT forest on Si/SiO_2 wafer transferred)	1 M H_2SO_4	Difficult (Not mentioned)	[S5]
Single-walled carbon nanotube	Oxidative cleavage of the C-C bond	GCE[a)] (Drop casting)	0.5 M H_2SO_4	Difficult (2.5 μg)	[S6]
Multi-walled carbon nanotube	Dopant-specific unzipping	GCE[a)] (CNT forest on Si/SiO_2 wafer transferred)	1 M H_2SO_4	Difficult (Not mentioned)	[S7]
Single-walled carbon nanotube	Oxidative cleavage of the C-C bond	GCE[a)] (Drop casting)	0.5 M H_2SO_4	Difficult (5 μg)	[S8]
Multi-walled carbon nanotube	Intercalation	MWCNT powder on membrane	18 M H_2SO_4	Good (50 mg)	**This work**

[a)](GCE; Glassy carbon electrode.)

Table S2. The concentration of Fe element is determined by ICP-MS measurement. Samples for ICP-MS analysis were prepared according to the following procedure. To obtain sample 1, 15 mg of the MWCNT powder was dispersed in concentrated sulfuric acid (30 mL) for 2 days and the mixture was separated from the solution by centrifugation (10 min at 6000 rpm). Then, the supernatant was diluted by deionized water (v/v = 1:100). For comparison, sample 2 was prepared by galvanostatic charging at a current density 0.5 mA cm^{-2} for 0.5 h using a three-electrode cell. The rest of the procedures was the same as described above.

Sample	Fe [ppb; µg kg^{-1}]
1. MWCNT: 2 days	6.8
2. MWNCT: charge state-*i*	10.9

Table S3. The full width at half maximum (FWHM) of the pristine MWNCT and all products was evaluated from the width of (002) peak using MDI Jade 6 software for multiple Gaussian function. A wider value of FWHM (B_{size}, °) indicates that the oxidation of MWCNT decreased the degree of crystallinity.

Sample	FWHM B_{size} [°]
1. MWCNT	0.68
2. unzipped MWCNT-*i*	1.14
3. GNR-2.5H	1.29
4. GNR-4H	1.41
5. GNR-7H	1.53

Table S4. The sheet resistance of the samples was investigated by a four-point probe measurement. This shows that the level of oxidation affects the conductivity of products.

Sample	Sheet resistance [Ω sq^{-1}]
1. MWCNT film	18.19
2. GNR-2.5H film	35.46

Table S5. Comparison of reported experimental methods with our electrochemical intercalation synthesis.

Types of CNT	Mechanism	Reagents	Synthesis method	Explosive /Toxicity	Ref
Multi-walled carbon nanotube	Edge-selective oxidation	HNO_3 vapor	Hydrothermal for HNO_3 vapor splitting	Both	[S9]
Single-walled or Multi-walled carbon nanotubes	Fluorination of CNT	EMIM BF4 ionic liquid	Microwave irradiation	Toxic	[S10]
Multi-walled carbon nanotube	Microwave interaction	H_2SO_4, H_3PO_4 and $KMnO_4$	Microwave irradiation	Both	[S11]
Multi-walled carbon nanotube	Atomic H-induced unzipping	Mixture of H_2, H_2O, CH_4 gas	Heat treatment at 850 ˚C	Explosive	[S12]
Multi-walled carbon nanotube	Surface oxidation	PmPV and DEC	Sonication with pre-treated MWCNT	None	[S13]

Multi-walled carbon nanotube	Mechano-chemical	-	Grinding with pre-treated MWCNT	None	[S14]
Multi-walled carbon nanotube	Intercalation	$KMnO_4$ and H_2SO_4	Solution reaction	Both	[S15]
Multi-walled carbon nanotube	Intercalation	$KMnO_4$, $NaNO_3$ and H_2SO_4	Solution reaction	Both	[S16]
Multi-walled carbon nanotube	Intercalation	$LiAlH_4$ and liquid NH_3	Solution reaction	Explosive	[S17]
Multi-walled carbon nanotube	Electrical break down	-	Electrical bias	None	[S18]
Multi-walled carbon nanotube	Intercalation	Potassium vapor	Heat treatment at 250 ˚C	Explosive	[S19]
Multi-walled carbon nanotube	Intercalation	18 M H_2SO_4 (no oxidizing agents)	Electrochemical reaction	None	**This work**

References

[S1] P. C. Eklund, C. H. Olk, F. J. Holler, J. G. Spolar and E. T. Arakawa, *J. Mater. Res.*, 1986, **1**, 361–367.

[S2] F. Beck, J. Jiang and H. Krohn, *J. Electroanal. Chem.*, 1995, **389**, 161–165.

[S3] A. Metrot and J. E. Fischer, *Synth. Met.*, 1981, **3**, 201–207.

[S4] D. B. Shinde, J. Debgupta, A. Kushwaha, M. Aslam and V. K. Pillai, *J. Am. Chem. Soc.*, 2011, **133**, 4168–4171.

[S5] S. P. Sasikala, T. Yun, D. S. Choi and M. S. Jeong, *ACS Appl. Mater. Interfaces*, 2019, **11**, 41, 38006-38015.

[S6] J. Debgupta, D. B. Shinde and V. K. Pillai, *Chem. Commun.*, 2012, **48**, 3088–3090.

[S7] J. Lim, U. N. Maiti, N. Y. Kim, R. Narayan, W. J. Lee, D. S. Choi, Y. Oh, J. M. Lee, G. Y. Lee, S. H. Kang, H. Kim, Y. H. Kim and S. O. Kim, *Nat. Commun.*, 2016, **7**, 1–9.

[S8] R. John, D. B. Shinde, L. Liu, F. Ding, Z. Xu, C. Vijayan, V. K. Pillai and T. Pradeep, *ACS Nano*, 2014, **8**, 234–242.

[S9] M. Yang, L. Hu, X. Tang, H. Zhang, H. Zhu, T. Fan and D. Zhang, *Carbon*, 2016, **110**, 480–489.

[S10] S. Vadahanambi, J. H. Jung, R. Kumar, H. J. Kim and I. K. Oh, *Carbon*, 2013, **53**, 391–398.

[S11] C. L. Sun, C. T. Chang, H. H. Lee, J. Zhou, J. Wang, T. K. Sham and W. F. Pong, *ACS Nano*, 2011, **5**, 7788–7795.

[S12] X. Fan, Z. Peng, Y. Yang, H. Zhou and X. Guo, *J. Mater. Chem. A*, 2015, **3**, 10077–10084.

[S13] L. Jiao, X. Wang, G. Diankov, H. Wang and H. Dai, *Nat. Nanotechnol.*, 2010, **5**, 321–325.

[S14] M. A. Kabbani, C. S. Tiwary, P. A. S. Autreto, G. Brunetto, A. Som, K. R. Krishnadas, S. Ozden, K. P. Hackenberg, Y. Gong, D. S. Galvao, R. Vajtai, A. T. Kabbani, T. Pradeep and P. M. Ajayan, *Nat. Commun.*, 2015, **6**, 1–8.

[S15] D. V. Kosynkin, A. L. Higginbotham, A. Sinitskii, J. R. Lomeda, A. Dimiev, B. K. Price and J. M. Tour, *Nature*, 2009, **458**, 872–876.

[S16] B. Xiao, X. Li, X. Li, B. Wang, C. Langford, R. Li and X. Sun, *J. Phys. Chem. C*, 2014, **118**, 881–890.

[S17] A. G. Cano-Márquez, F. J. Rodríguez-Macías, J. Campos-Delgado, C. G. Espinosa-González, F. Tristán-López, D. Ramírez-González, D. A. Cullen, D. J. Smith, M. Terrones and Y. I. Vega-Cantú, *Nano Lett.*, 2009, **9**, 1527–1533.

[S18] K. Kim, A. Sussman and A. Zettl, *ACS Nano*, 2010, **4**, 1362–1366.

[S19] D. V. Kosynkin, W. Lu, A. Sinitskii, G. Pera, Z. Sun and J. M. Tour, *ACS Nano*, 2011, **5**, 968–974.